



# TiO<sub>2</sub> and TiO<sub>2</sub>–SiO<sub>2</sub> coated cement: Comparison of mechanic and photocatalytic properties



C. Mendoza<sup>a</sup>, A. Valle<sup>a</sup>, M. Castellote<sup>b</sup>, A. Bahamonde<sup>a,\*</sup>, M. Faraldos<sup>a,\*</sup>

<sup>a</sup> Instituto de Catálisis y Petroleoquímica, ICP-CSIC, C/ Marie Curie 2, 28049 Madrid, Spain

<sup>b</sup> Instituto de Ciencias de la Construcción Eduardo Torroja, CSIC, C/ Serrano Galvache 4, 28033 Madrid, Spain

## ARTICLE INFO

### Article history:

Received 11 July 2014

Received in revised form 9 September 2014

Accepted 20 September 2014

Available online 13 October 2014

### Keywords:

Photocatalysis

TiO<sub>2</sub>

SiO<sub>2</sub>

NO<sub>x</sub>

RhB

## ABSTRACT

An increasingly known application of nanomaterials in the construction industry is related to the photoactivity ability of semiconductors, where nano-anatase TiO<sub>2</sub> is perhaps the most well-known photocatalytic semiconductor and one which possesses a strong oxidizing capability. To analyze the photo-efficiency of four TiO<sub>2</sub> coatings and the effect of SiO<sub>2</sub> interlayer on the mechanic and photocatalytic activity in Rhodamine B (RhB) and NO<sub>x</sub> photodegradation, two photocatalytic cement series have been prepared. First, cement mortar was coated with three commercial TiO<sub>2</sub> suspensions (GG1, GC7 and CG13) and a home-made titania sol–gel (TEA), and secondly an insertion of a SiO<sub>2</sub> layer was applied on cement surface before spraying the TiO<sub>2</sub> layer.

All studied TiO<sub>2</sub>-cements exhibited a significant RhB and NO<sub>x</sub> photodegradation, arising almost total RhB molar conversions, and upper 53% for NO<sub>x</sub> photo-oxidation respectively. Nevertheless, although SiO<sub>2</sub> layer deposited in between mortar and TiO<sub>2</sub>-cement did not stabilize the commercial TiO<sub>2</sub> coatings, a good adhesion was observed when silica was applied joint to the home-made titania gel (TEA), probably as a consequence of the interactions encountered between SiO<sub>2</sub> and TiO<sub>2</sub> gels. CG7-Si-Cem exhibited high rate at shorter irradiation times, but TEA-Cem and TEA-Si-Cem can be considered as very interesting and potential photocatalytic mortars due to useful mechanical properties, with a very good coatings adhesion that provides promising outdoor use, and good photo-efficiencies in RhB and NO<sub>x</sub> photo-oxidation.

© 2014 Elsevier B.V. All rights reserved.

## 1. Introduction

Air quality has gone continuously degrading along the last century due to high population, industrial activities and gasoline and diesel engines which have caused an important damage in urban environments [1]. Despite regulation straightening [2], air pollutants concentration is even so one of the biggest problems that modern society faces increasingly aware of the danger associated. Among air pollutants, ozone, particulate matter, ammonia, NO<sub>x</sub>, CO and VOCs are the most dangerous due to their direct impact on human health, environmental damage and potential reactivity [3]. It can be emphasized NO<sub>2</sub> gas-like NO as the major air pollutant that threatens human health and also participates in the formation of photochemical smog and ozone [4], contributing to climate change as well.

Some measures are frequently assumed by big cities authorities to fight traffic and other emission sources in order to control the emissions levels or apply improved technology to reduce air contamination: green-fuels, electric vehicles, filters, adsorbents, photocatalytic urban furniture, etc. in order to get the abatement and/or remediation of urban air. In this context, solar assisted heterogeneous photocatalysis has demonstrated to be a potential alternative to air pollution control [5]. Recently, a promising approach for solving the problems caused by NO<sub>x</sub> involves the use of photochemical conversion of nitrogen oxides to nitrates, due to these heterogeneous photocatalytic oxidation (PCO) processes. The products of the reaction are in the form of water-soluble nitrate compounds that can be washed from the active concrete surfaces by rain. Therefore, one proposed way of reducing the NO<sub>x</sub> and VOCs concentration in the atmosphere is the use of titanium dioxide in construction materials, near to mobile sources such as photocatalytic cement infrastructures or concrete roads [6,7].

In this sense an increasingly known application of nanoparticles and nanoporous materials in the construction industry is related to the photocatalytic ability of semiconductors materials [8,9], where nano-anatase TiO<sub>2</sub> is perhaps the most well-known

\* Corresponding author. Tel.: +34 915854820; fax: +34 915854760.

\*\* Corresponding author. Tel.: +34 915855475; fax: +34 915854760.

E-mail addresses: [abahamonde@icp.csic.es](mailto:abahamonde@icp.csic.es) (A. Bahamonde), [mfaraldos@icp.csic.es](mailto:mfaraldos@icp.csic.es) (M. Faraldos).

photocatalytic semiconductor and one which possesses a strong oxidizing capability. Incorporating nanoparticles of anatase is one pathway towards nano-engineering of cement-based materials. In addition to imparting self-cleaning and photocatalytic properties, a few studies have shown that nano-TiO<sub>2</sub> can accelerate the early-age hydration of portland cement, improve compressive and flexural strengths, and enhance the abrasion resistance of concrete [10]. Indeed, nanoparticles can impart novel properties self-sensing, pollution abatement, and self-cleaning ability as well as modifying cement hydration behaviour. In this regard, the use of nanosilica particles have given place to an important increase in the compression strength of cement pastes [11], improvement of photocatalytic [12–14] and self-cleaning properties [15], at the same time that other types of nanoparticles (nanotubes, nanofibers, or nanoclay) are also responsible for a higher hydration degree of cementitious compounds as long as higher nanoparticle dispersion can be achieved [16].

Previous studies [17,18] have indicated that construction materials containing TiO<sub>2</sub>, when exposed to sunlight, can effectively oxidize the pollutants adsorbed on their surfaces, indicating, besides, “self-cleaning” properties [10]. To verify self-cleaning performances of photocatalytic-cementitious materials or concretes, several test involving organic substances have been set up mainly based on the degradation of colour in dyes such as Rhodamine B (RhB) test [19].

Usually, the photocatalytic oxidation reactions happen in the presence of water, oxygen, and under UV or near-UV light [20] which enable nano-titania to oxidize or decompose some pollutants [21]. Therefore, when TiO<sub>2</sub> photocatalyst is exposed to UV rays it triggers the catalytic reaction to oxidize the organic and inorganic substances. Although some authors [10] mentioned that air pollution reduction depends on the UV intensity, visible light still allows acceptable degradation rates.

During last decades the development of new photoactive building materials has woken up an enormous interest among urban and scientific communities, but advances slowed down after titania was introduced in different ways (spraying, mixing, intercalation, etc.) [10], and no much effort has been made in the published literature related to effect of multiple reaction parameters and durability and mechanical strength of obtained photocatalytic-infrastructure materials [22]. Titania coatings are generally layers of around 200 nm of thickness [23], which are deposited using some techniques, such as sputtering [24], electrophoretic deposition [25], spray pyrolysis [26], thermal oxidation [27], chemical vapor deposition [28] and wet coating [29], among the main reported methodologies.

Nowadays, the target is to obtain more active photocatalysts and more stable when applied over urban infrastructures to assure the durability and reduce maintaining costs. Commercial sprayable photo-catalytic suspensions contain some additives to guarantee the perdurability, but sometimes a detrimental effect over photocatalyst properties is consequently caused.

In this context, the principal aim of this study has consisted in the application of titania and titania-silica coatings on mortars, the modification if any, produced on original mechanic properties and their behaviour presented on the degradation of NO<sub>x</sub> and Rhodamine B (RhB) to assess their photocatalytic efficiencies.

## 2. Experimental

### 2.1. Materials

Cement mortar was constituted by cement: sand: water in 1:3:0.5 ratio. Samples were cured for 28 days on a chamber

under saturated humidity environment. Three commercial and one home-made TiO<sub>2</sub> suspensions were used to build up the photocatalytic coating. Commercial TiO<sub>2</sub> suspensions were supplied by Cristal Global: S5-300A (CG1), PC-S7 (CG7) and S5-300B (CG13), and a homemade titania sol (TEA) was prepared by titanium isopropoxide hydrolysis in acid media, maintained stirring during three days to achieve complete peptization and further purification by sequential dialysis treatment with acidic (pH 2.5–3) Milli-Q water until a stabilized suspension was obtained [30].

The TiO<sub>2</sub> sols were sprayed over mortar surface and dried at room temperature overnight; the prepared photocatalytic cements were designated as catalyst name-Cem: CG1-Cem, CG7-Cem, CG13-Cem and TEA-Cem.

Afterwards, a SiO<sub>2</sub> suspension was synthesized by hydrolysis of tetraethylorthosilicate in acid media, the mix was stirred over 24 h until complete peptization was reached [31] and a stable suspensions obtained. This SiO<sub>2</sub> sol was applied on cement surface previously to spray the TiO<sub>2</sub> layer and dried at room temperature overnight. Later, the TiO<sub>2</sub> photocatalytic layers were coated generating a new photo-cements family, systematically named as catalyst-Si-Cem: CG1-Si-Cem, CG7-Si-Cem, CG13-Si-Cem and TEA-Si-Cem.

### 2.2. Characterization

The catalysts and coated cements were physico-chemically characterized: X-ray diffraction (XRD), UV–Vis Diffuse Reflectance spectroscopy (DRS), Inductively Coupled Plasma Emission Spectroscopy (ICP-OES), helium pycnometry, N<sub>2</sub> adsorption–desorption isotherms, mercury intrusion porosimetry (MIP), NH<sub>3</sub> chemisorption, scanning electron microscopy (SEM), scanning electron microscopy coupled to back scattered electron detector (SEM-BSE) and transmission electron microscopy (TEM), in order to understand the most relevant catalysts and support properties and the modification suffered after immobilization.

Powder XRD patterns of catalysts xerogels and photo-cements were obtained with a PANalytical X'Pert operating at 45 kV and 40 mA that uses an X'Celerator detector and nickel-filtered Cu K $\alpha$  radiation. The diffractograms were acquired between 4 and 90°, 0.04° step size and accumulation time of 20 s per point. Crystallite size was calculated employing the Scherrer equation [32], and the crystalline phases were identified by comparison with ICDD PDF database.

The specific surface areas and mesopore size distribution of xerogels, mortars and coated mortars were determined by the BET method as of N<sub>2</sub> isotherm data measured at 413 K in a Micromeritics ASAP 2420. Porosity study was completed by mercury intrusion porosimetry in a Micromeritics AutoPore IV 9520. Total pore volume was evaluated combining both techniques.

Mortar and coated-mortar samples density were determined by helium pycnometry on a Micromeritics Accupyc 1340.

Ammonia adsorption at room temperature, measured on an ASP-2010 C instrument (Micromeritics), was used to evaluate surface acidity of titania xerogels. The samples were first outgassed at 350 °C for 2 h, and then cooled to 30 °C before determining the overall adsorption capacity (physisorption plus chemisorption). Subsequently, after outgassing the samples at 30 °C for 4 h to remove the physisorbed molecules, a second adsorption process was carried out in order to obtain the chemisorbed amount by difference between the two isotherms.

The UV-Vis diffuse reflectance spectra were recorded in a UV-Visible Agilent-Varian, Cary 5000, equipped with an integrating sphere. Analyses of the band gap transitions of the samples were made using equations developed elsewhere [33,34].

The elemental composition of commercial and prepared  $\text{TiO}_2$  suspensions were determined by ICP-OES, Perkin Elmer, model Optima 3300 DV.

The catalysts particles size and morphology were studied by Transmission Electron Microscopy (TEM) JEOL 2100F, with a resolution of 0.19 nm [35]; and their local composition was verified by Energy Dispersive X-Ray Spectrometry (EDXS) INCA x-sight by Oxford Instruments.

The structural and morphological study was completed at micrometric level to go deeper on  $\text{TiO}_2$  particles surface, size and shape knowledge; for this purpose a Scanning Electron Microscope (SEM) Hitachi Tablet Microscope TM-1000 coupled to an EDX analyzer (SwiftED, Oxford Instruments) was used.

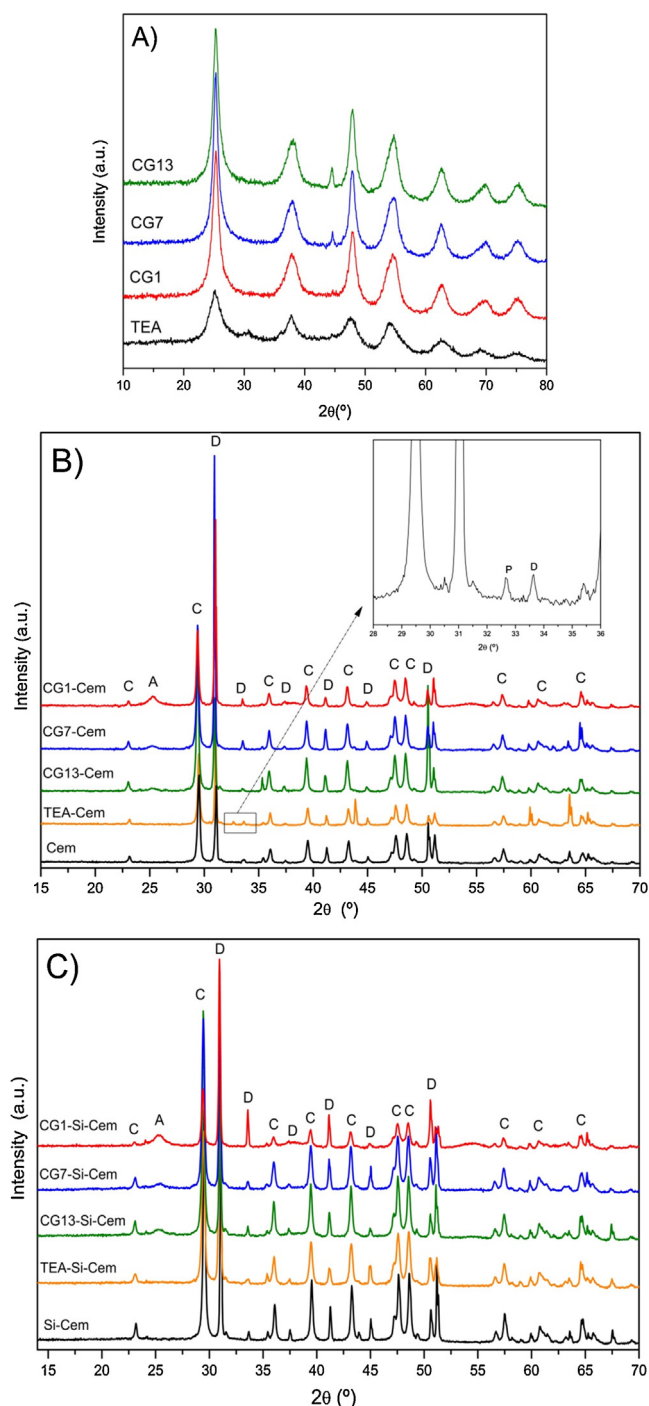
A Back-Scattering Electron detector coupled to a Hitachi S-4800 SEM (BSE-SEM) was employed to study thickness, homogeneity and continuity of  $\text{SiO}_2$  and/or  $\text{TiO}_2$  layers as well as mortar features. For that purpose, a 1 cm cross section of each sample was embedded in resin, dried at room temperature, then polished and outgassed before analysis.

Coating adhesion studies were performed following cross cut adhesion tests on every prepared photocement. Several cross cuts were made on the samples surface with a standard cutter, then, the scratched surfaces were observed by SEM and the micrographs obtained were qualitatively analyzed.

### 2.3. Photocatalytic activity

Photocatalytic activity runs to evaluate the RhB photodegradation were carried out in a chamber with an inner surface covered by reflective metal sheets and equipped with six fluorescent lamps (4 BLB and 2 Daylight, 15w each) located at the top side of the chamber that provide  $30 \text{ W m}^{-2}$  of irradiance. Following an adapted version of UNI 11259:2008 standard [36], a volume of 1.5 mL of  $10^{-4} \text{ M}$  RhB was deposited on mortar surfaces, describing a circular homogeneous spot with  $1.56 \times 10^{-4} \text{ moles m}^{-2}$  RhB surface concentration, then the samples were left in the dark over 24 hr to allow drying of solvent and dye adsorption. Photodegradation evolutions were followed by measuring the RhB spots discoloration as UV-Vis diffuse reflectance at different irradiation time intervals from 0 and 5 days. The percentage of photodegradation was calculated as  $[(A_0 - A_i)/A_0] \times 100$ , where  $A_0$  is the integrated area of the mean peak of RhB at  $\lambda = 554 \text{ nm}$  corresponding to initial time (after the 24 h of drying and adsorption period), while  $A_i$  corresponds to the integrated peak area at reaction time  $i$ , that was quantified after deconvolution of UV-Vis diffuse reflectance (DRS) peak doublet and disregard the shoulder contribution at lower wavelength with the aim to minimize other non-photocatalytic mechanism of RhB degradation [37–39]. The relationship between the DRS peak area and the concentration obeys the equation  $F(R) = (1 - R)^2 / 2R \propto \varepsilon \cdot C / s$ , where  $F(R)$  is the Kubelka-Munk function,  $R$  the diffuse reflectance,  $\varepsilon$  is the molar absorptivity coefficient,  $C$  is the RhB concentration and  $s$  is the scattering coefficient [40].

Nitrogen oxides photodegradation runs were carried out in a photoreactor system that obeys UNI 11247:2010 [41] requirements: A 300 W Osram Ultravitalux lamp ( $\lambda_{\text{Max}} = 365 \text{ nm}$ ) that provides  $20 \text{ W m}^{-2}$  of irradiance on concrete surface was used. The sample, with an exposed size of  $64 \text{ cm}^2$ , was settled in a 2.81 L and 13.5 cm height Pyrex reactor. Inlet  $\text{NO}_x$  concentration was  $0.55 \pm 0.05 \text{ mg L}^{-1}$  ( $0.4 \text{ mg L}^{-1} \text{ NO} + 0.15 \text{ mg L}^{-1} \text{ NO}_2$ ) at a constant  $1.5 \text{ L min}^{-1}$  flow. Photoreactor was provided with three mass flow and temperature controllers (Brooks model 5850S). The photodegradation reactions were carried out at the temperature  $303 \pm 5 \text{ K}$ . Inlet and outlet nitrogen oxides ( $\text{NO}$  and  $\text{NO}_2$ ) concentrations were analyzed by chemiluminescence in a  $\text{NO}/\text{NO}_x$  analyzer model AC32M Environment.



**Fig. 1.** Diffractograms of (A)  $\text{TiO}_2$  xerogels, (B)  $\text{TiO}_2$ -Cem and (C)  $\text{TiO}_2$ -Si-Cem (crystalline phases identification: C: calcite, D: dolomite, A: anatase, P: Ca, Ti mix oxide perovskite type).

## 3. Results and discussion

### 3.1. Characterization studies

The XRD patterns of all studied catalysts-coated materials are displayed in Fig. 1. Dolomite and calcite, as expected, were the majoritarian phases observed for mortar samples, while anatase was the unique crystalline phase identified on the four titanium oxide xerogels. The sum of these phases was mainly detected on catalyst-coated and catalyst-Si-coated mortar specimens, only in the case of TEA-Cem a low intensity well-defined peak at

**Table 1**  
Main physico-chemical properties of TiO<sub>2</sub> catalysts.

	pH <sup>a</sup>	TiO <sub>2</sub> <sup>a</sup> (wt%)	S <sub>BET</sub> <sup>b</sup> (m <sup>2</sup> ·g <sup>-1</sup> )	V <sub>mesopore</sub> <sup>b</sup> (cm <sup>3</sup> ·g <sup>-1</sup> )	d <sub>pore</sub> <sup>b</sup> (nm)	Density <sup>b</sup> (g·cm <sup>-3</sup> )	d <sub>crystallite</sub> <sup>b</sup> (nm)	Acidity <sup>b</sup> (mmol H <sup>+</sup> ·g <sup>-1</sup> )	BG <sup>b</sup> (eV)
CG1	1 ± 0.2	20 ± 2	350 ± 20	0.38 ± 0.02	5.5 ± 0.3	3.1 ± 0.01	6.6 ± 0.2	2.4 ± 0.05	3.38 ± 0.03
CG7	8 ± 0.3	10 ± 1	270 ± 15	0.36 ± 0.02	7.0 ± 0.3	2.7 ± 0.01	8.6 ± 0.3	0.8 ± 0.02	3.39 ± 0.03
CG13	13 ± 0.3	18 ± 2	340 ± 20	0.53 ± 0.03	10.0 ± 0.5	2.9 ± 0.01	7.4 ± 0.3	0.7 ± 0.01	3.35 ± 0.03
TEA	3 ± 0.2	20 ± 2	340 ± 20	0.24 ± 0.01	2.3 ± 0.2	2.8 ± 0.01	3.8 ± 0.2	1.3 ± 0.03	3.72 ± 0.04

<sup>a</sup> Parameters measured on catalyst suspension.

<sup>b</sup> Parameters measured on catalysts xerogels.

2 theta = 32° could be identified as being compatible with a perovskite-type calcium-titanium mix oxide, that could indicate a stronger interaction between TiO<sub>2</sub> and mortar components. In the case of TEA coated mortars, the anatase XRD peaks were almost inappreciable, that corresponds to the small crystallite size (see Table 1) and well dispersed layer.

Table 1 summarizes the main physico-chemical properties of the studied titania photocatalysts, and in Table 2 are given the main physico-chemical properties of raw and coated-mortars.

Whereas the commercial TiO<sub>2</sub> presented anatase crystallite sizes between 6.6 and 8.6 nm, the home-made titania (TEA) was constituted by smaller anatase crystallites (3.8 nm).

The band gap of catalysts and catalysts-coated mortars (see Tables 1 and 2) were the same while a lower energy was observed for previously SiO<sub>2</sub> coated mortars, higher in the cases of acidic pH TiO<sub>2</sub> sols (CG1 and TEA) used. The lowering could be probably due to the coexistence of two oxides capable to interfere in the neighbour electronic system [42], what should conduce to better photoefficiency.

All titania suspensions presented around a 20 wt.% of TiO<sub>2</sub>. The different pH values of titania suspension could affect the way to bond with the cementitious materials, probably leading to some different surface properties affecting their final mechanical and adhesion features. While the home-made titania catalyst suspension has a very acid pH value (3), in the same range than pH value of CG1 titania (1), CG7 suspension was stabilized at pH 8 and a very basic value (13) was observed in CG13 TiO<sub>2</sub>.

It is known that the surface acidity can depend on the preparation method and sample preconditioning employed in each case. In this sense, shifts in catalyst surface acidity can occur in response to changes in cation coordination, crystallinity, hydration state, surface composition and structural charge or ion exchange capacity, among others. These factors can be invoked to explain the relatively high surface acidity observed for CG1 and TEA samples, especially in the case of CG1 titania suspension with a very acid pH (see Table 1).

On the other side, N<sub>2</sub> adsorption-desorption isotherms for all studied titania samples correspond to type IV with a H2 hysteresis loop type, typical of many inorganic oxide gels [43] (not show here). The pore structures in these materials are usually complex

and tend to be made up by interconnected networks of pores of different size and shape, being the H2 hysteresis loop characteristic for mesoporous materials consisting of spherical particles, with a relative wide pore size distribution and a pore shape that is often described as “ink bottle”-type [44]. A microporosity contribution was found for all TiO<sub>2</sub> xerogels. Therefore, the pore size distribution for the four titania samples are described in the range of micro-mesoporosity. Whereas the home made TEA titania presented the lowest mesopore volume and diameter (very close to micropores), CG13 titania with a very basic pH, showed the largest mesopore volume and diameter. In all cases very high surfaces areas around 300 m<sup>2</sup> g<sup>-1</sup> were always found as correspond to micro-mesoporous titanias, optimal to provide enough adsorption sites to star up the catalytic process. Although appreciable mesoporosity was found for all studied titanium dioxides xerogels, some differences are apparent among them which can affect their pore network and chemical structure. An increase in the pH of the synthesis generally leads to enhanced ligand displacement and consequently to the development of hydroxo and oxo bridges between neighbouring cations, and ultimately to cementation particles [45] without introducing in this case important changes in its textural structure. This could explain the slightly higher mesoporosity developed by the TiO<sub>2</sub> sample CG13. Finally, no important differences were observed when their densities were compared, always around 3 g cm<sup>-3</sup> for all TiO<sub>2</sub> xerogels.

The reference mortar specific surface area was 6.2 m<sup>2</sup> g<sup>-1</sup>, and exhibited 28.5% porosity with a 700 nm maximum pore size distribution (Table 2). The textural properties of coated mortars were not much altered when compared to original cementitious material, and fundamentally presented a macroporosity as correspond to the lower S<sub>BET</sub> observed. A very slight increment of surface area appreciated when titania coatings were deposited on mortar surface could be due to nano-TiO<sub>2</sub> layer porosity contribution. However, the insertion of the SiO<sub>2</sub> coating reduces this effect in the case of CG1 and CG7-Cem, remaining almost equal or slightly higher S<sub>BET</sub> in TEA and the CG13 coated mortars. Likewise, slightly higher densities were measured associated to a wider maximum pore diameter. In this sense, the main change was observed in pore size distribution were a shift to wider macropore diameter was detected for all

**Table 2**  
Main physico-chemical properties of reference and coated-mortars.

	S <sub>BET</sub> (m <sup>2</sup> g <sup>-1</sup> )	V <sub>total pore</sub> (cm <sup>3</sup> g <sup>-1</sup> )	Porosity (%)	d <sub>p,max</sub> (nm)	Density (g·cm <sup>-3</sup> )	BG (eV)	TiO <sub>2</sub> layer thickness (nm)	SiO <sub>2</sub> layer thickness (nm)
Cem	6.2 ± 0.3	0.16 ± 0.01	28.5 ± 1.5	700 ± 30	2.72 ± 0.01	–	–	–
Si-Cem	5.5 ± 0.3	0.16 ± 0.01	29.4 ± 1.6	850 ± 40	2.73 ± 0.01	–	–	–
CG1-Cem	7.9 ± 0.4	0.15 ± 0.01	30.2 ± 1.7	1100 ± 55	2.75 ± 0.01	3.38 ± 0.03	2600 ± 300	–
CG7-Cem	7.3 ± 0.3	0.16 ± 0.01	31.3 ± 1.7	950 ± 30	2.76 ± 0.01	3.39 ± 0.03	800 ± 100	–
CG13-Cem	6.8 ± 0.3	0.15 ± 0.01	28.8 ± 1.5	840 ± 40	2.73 ± 0.01	3.35 ± 0.03	1800 ± 200	–
TEA-Cem	7.2 ± 0.4	0.15 ± 0.01	28.9 ± 1.5	730 ± 35	2.73 ± 0.01	3.72 ± 0.04	640 ± 50	–
CG1-Si-Cem	5.4 ± 0.3	0.15 ± 0.01	26.8 ± 1.4	1040 ± 50	2.75 ± 0.01	3.27 ± 0.03	750 ± 100	n.a.
CG7-Si-Cem	5.6 ± 0.2	0.16 ± 0.01	30.0 ± 1.6	790 ± 40	2.76 ± 0.01	3.32 ± 0.03	1500 ± 200	1500 ± 200
CG13-Si-Cem	7.5 ± 0.3	0.16 ± 0.01	29.7 ± 1.6	790 ± 40	2.74 ± 0.01	3.33 ± 0.03	1500 ± 200	900 ± 100
TEA-Si-Cem	6.9 ± 0.3	0.14 ± 0.01	28.1 ± 1.5	750 ± 35	2.73 ± 0.01	3.62 ± 0.04	450 ± 50	n.a.

n.a.: non appreciated.



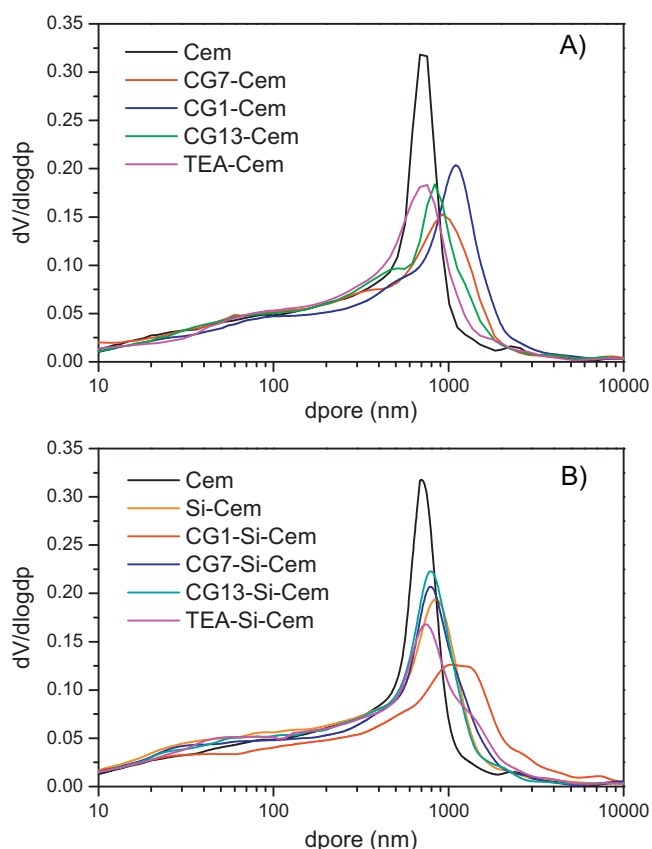


Fig. 2. Pore size distribution of (A)  $\text{TiO}_2$ -Cem and (B)  $\text{TiO}_2$ -Si-Cem.

commercial  $\text{TiO}_2$ -cements (Fig. 2A), more significant in the case of acidic pH commercial catalysts coatings (CG1) that could implies a partial dissolution of some mortar components [46,47], meanwhile TEA-cem barely modifies raw mortar (Cem) textural properties and only a slight pore volume decrease was observed.

A similar behaviour presented previously  $\text{SiO}_2$  coated mortars (Fig. 2B), where only CG1-Si-Cem modifies its maximum pore size, with erosions probably due to the acidic attack [38]. In the case of the other catalysts coatings (TEA, CG7 and CG13-Si-Cem)  $\text{SiO}_2$  looks to act as a protective layer that preserves raw cement characteristics [48].

The surface of coated mortars presents scratches when observed at SEM, Fig. 3 upper shows that these scratches are generalized on commercial  $\text{TiO}_2$  coated cements (Fig. 3a–c, upper) and produces even peeling out of outer titania layer in the case of  $\text{TiO}_2$ -Si-Cem. On the contrary, TEA-Cem exhibits a very homogeneous surface with no scrapes that resulted altered when  $\text{SiO}_2$  layer was previously coated (Fig. 4d, upper) although no peeling out was observed and the scratches are not as deep as those presented on CG1, CG7 and CG13-Si-Cem surfaces (Fig. 4a–c, upper side).

The layer thickness and interactions between catalysts and mortar were analyzed by SEM-BSE, and although the volume sprayed were calculated to provide a similar coating size, the commercial  $\text{TiO}_2$  catalysts were deposited in a thicker layer (2600–640 nm) (see Table 2); they were discontinuous and heterogeneous (Fig. 3a–c, down), by contrast, TEA coating was thin (Table 2) but continuous and homogeneous (Fig. 3d, down), besides the Ca, Ti mapping images (Fig. 3, down) point out that some kind of interaction could be taking place with the presence of  $\text{TiO}_2$  beyond the mortar surface, this observation agrees with the presence of a new minority crystalline phase identified as calcium-titanium mix oxide by XRD.

The insertion of a  $\text{SiO}_2$  layer in between mortar and titania coating produces a decrease in the thickness of  $\text{TiO}_2$  coatings (Table 2), except in the case of CG7-Si-Cem. Even more an intimate mixing of  $\text{SiO}_2$  and titania layer or mortar must happen because could not be distinguished when acid  $\text{TiO}_2$  (CG1 and TEA) was spread (Fig. 4a and d, respectively).

Micrographs obtained after adhesion test are displayed in Fig. 5. CG1-Cem showed a very poor union between photocatalyst coating and mortar support, even some scratches on cement surface are observed; probably do to CG1 suspension acidity (pH 1). CG7-Cem and, over all, TEA-Cem presented the best titania layer aspect, with minimum peeling around cuts. Therefore the qualitative observation of photoactive layer followed the quality order: TEA-Cem > CG7-Cem >> CG13-Cem >> CG1-Cem, as can be seen from Fig. 5d, b, c and a, respectively.

The  $\text{SiO}_2$  sol coating, in general, did not improve the adhesion of the photocatalyst layer, except in the case of TEA-Si-Cem in which a close interaction between  $\text{SiO}_2$  and  $\text{TiO}_2$  was observed in the micrographs (Fig. 5h). CG1-Si-Cem presented a surface with multiple erosion and partial layer lost. Intermediate situations were observed for CG7 and CG13-Si-Cem. Therefore the qualitative observation of photoactive layer over silica-coated mortar followed the quality order: TEA-Si-Cem >> CG7-Si-Cem > CG13-Si-Cem >> CG1-Si-Cem, as can be seen from Fig. 5h, f, g and e, respectively.

The good adhesion that TEA presented both with and without  $\text{SiO}_2$  interlayer, even if do not have a direct effect over photoefficiency, would provide, for the outdoor application, an associated durability enhancement that could be an appreciated property, avoiding the release of nanoparticles to environment.

### 3.2. Rhodamine B photodegradation

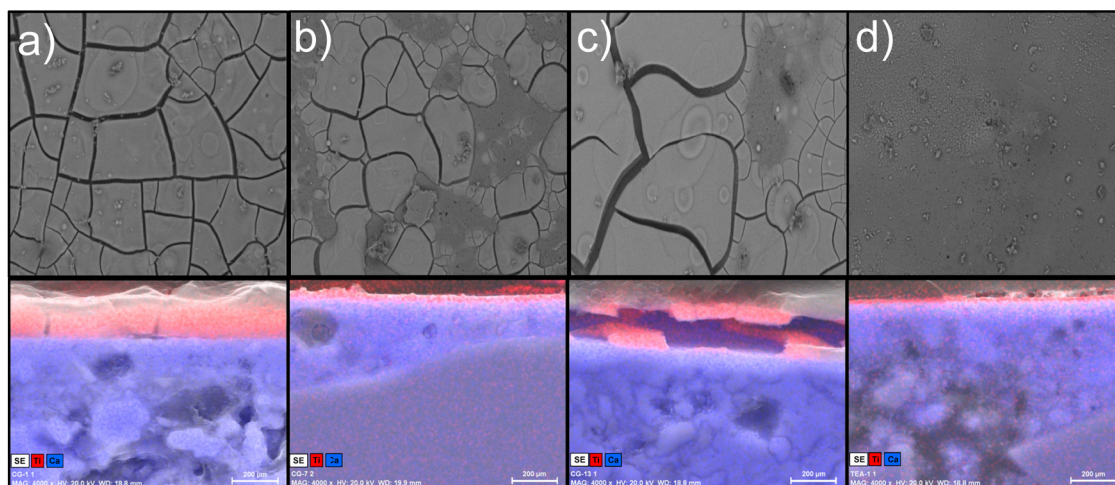
The micrographs of  $\text{TiO}_2$ -Cem and Cem reference surfaces that represent the bleaching evolution of RhB spots with irradiation times are given in Table 3, showing a quick look up on dye photodegradation evolution.

At initial irradiation time, as a preliminary observation, the DRS peak intensity of CG1-Cem is about 40% lower than the others coated mortars: CG7-Cem, CG13-Cem and TEA-Cem; that could be associated to a higher adsorption capacity due to the deep erosions produced on CG1-Cem mortar by the acidic catalyst coating [49], as previously described.

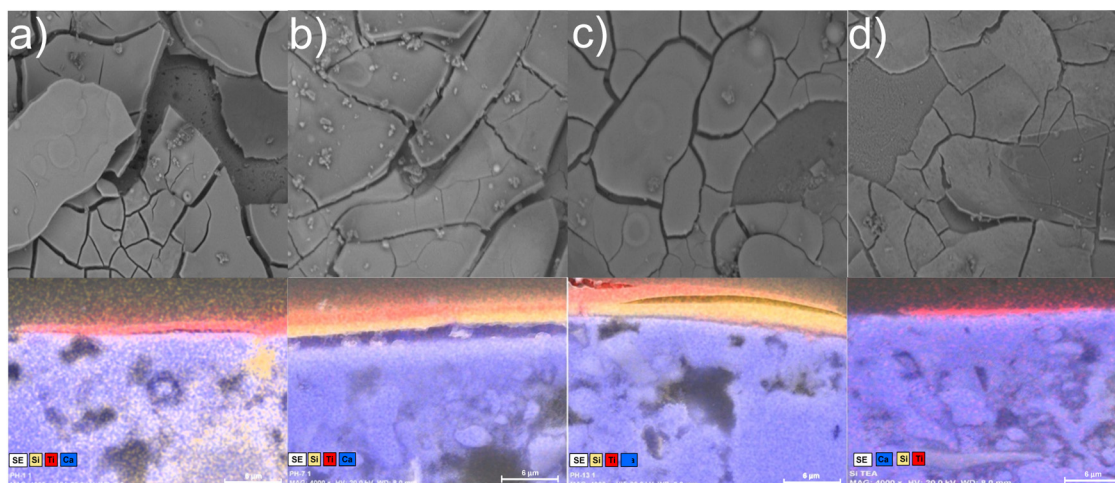
From Fig. 6, where the RhB photodegradation measured as surface decolouration by DRS for the four  $\text{TiO}_2$ -cements, at different irradiation times, could be determined that the fastest RhB photodegradation evolution corresponds to CG1-Cem that could be favoured by a lower initial concentration of RhB due to an important colourant adsorption and penetration to inner surfaces of mortar as a consequence of its highest macropore diameter (1100 nm). RhB photodegradation profiles change during reaction time, while CG1-Cem reaches practically total molar conversion at 1 day, CG7-Cem presents faster initial photo-oxidation rate. It can be emphasized that CG13-Cem and TEA-Cem needed an initial time to begin the photo-activation (photoinduction period). Nevertheless the four titania-coated mortars owned the capability to photodegrade completely RhB after five days of irradiation.

The fact that high initial reaction rate decreases rapidly with time makes difficult to adjust experimental points to a simple kinetic model, probably due to mixed degradation mechanisms and the formation of photoactive intermediates, as previously reported [50,51].

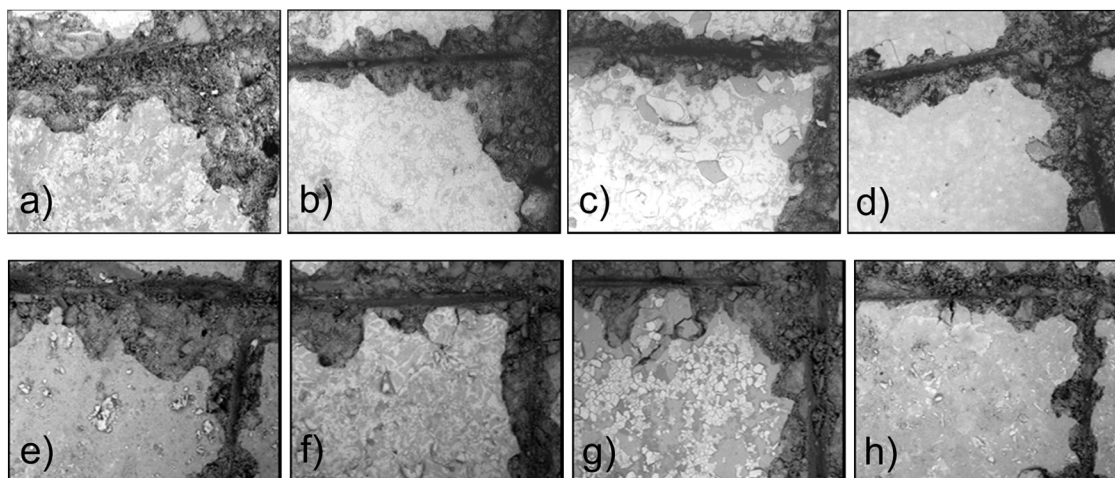
When a  $\text{SiO}_2$  sol interlayer was applied the DRS signal of all the coated mortars had similar intensities, but double higher than those presented by RhB spots at initial stage on  $\text{TiO}_2$ -Cem samples, which could be pointing out an equivalent adsorption capacity among all



**Fig. 3.** Micrographs of surface aspect (upper images, at 1000× magnification) and coating thickness (down) of TiO<sub>2</sub>-Cem: (a) CG1-Cem, (b) CG7-Cem, (c) CG13-Cem and (d) TEA-Cem. (Mapping: Ti (red) and Ca (blue)). (For interpretation of the references to color in this figure legend, the reader is referred to the web version of the article.)



**Fig. 4.** Micrographs of surface aspect (upper images, at 1000× magnification) and coating thickness (down) of TiO<sub>2</sub>-Si-Cem mortars: (a) CG1-Si-Cem, (b) CG7-Si-Cem, (c) CG13-Si-Cem and (d) TEA-Si-Cem. (Mapping: Ti (red), Si (yellow) and Ca (blue)). (For interpretation of the references to color in this figure legend, the reader is referred to the web version of the article.)

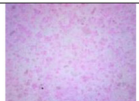
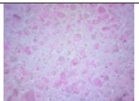
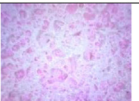
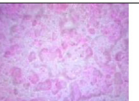
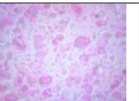
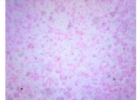
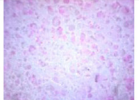
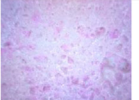

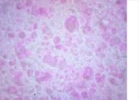
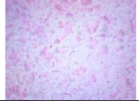
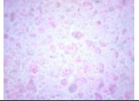
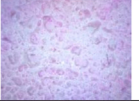
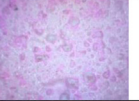
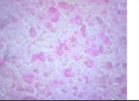
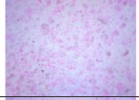
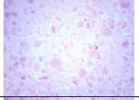

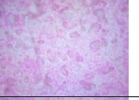
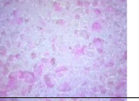
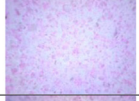
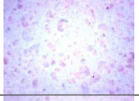

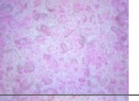

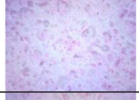

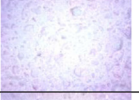
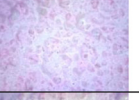
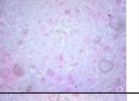
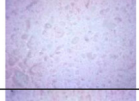
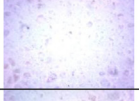

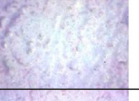
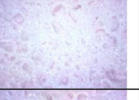
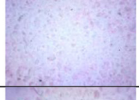



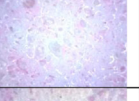
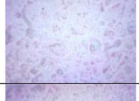


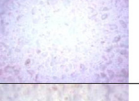








**Fig. 5.** Adhesion test micrographs (at 100× magnification) for TiO<sub>2</sub> catalysts coated mortars: (a) CG1-Cem, (b) CG7-Cem, (c) CG13-Cem, and (d) TEA-Cem. TiO<sub>2</sub>-SiO<sub>2</sub> coated mortars: (e) CG1-Si-Cem, (f) CG7-Si-Cem, (g) CG13-Si-Cem and (h) TEA-Si-Cem.



**Table 3**

Micrographs of RhB decolouration by photocatalytic degradation on TiO<sub>2</sub> coated cements, obtained after different irradiation times.

Time	Cem	CG1-Cem	CG7-Cem	CG13-Cem	TEA-Cem
0					
30 min					
60 min					
120 min					
240 min					
1 day					
2 days					
3 days					
4 days					
5 days					

SiO<sub>2</sub> coated cements but reduced into the mortar microstructure by the filling effect of SiO<sub>2</sub> [52–54]. The four samples: CG1-Si-Cem, CG7-Si-Cem, CG13-Si-Cem and TEA-Si-Cem showed a markedly lower RhB initial photodegradation rate as can be observed from Fig. 7, where RhB concentration evolution versus reaction time has been represented. The RhB spots bleaching evolution with irradiation times can be well followed by the micrographs sequences of TiO<sub>2</sub>-Si-Cem samples and reference presented in Table 4. While CG7-Si-Cem presented the fastest RhB reaction evolution, TEA-Si-Cem photoefficiency was the least affected comparing with the corresponding TiO<sub>2</sub>-Cem. This behaviour indicates that an initial activation stage, 4–6 h depending on the catalyst coating, looks necessary, after that photoinduction period [55], [56], CG1-Si-Cem, CG7-Si-Cem and TEA-Si-Cem reached >90% RhB conversion after 5 days, meanwhile CG13-Si-Cem activation period was longer and the conversion hardly reached 80%.

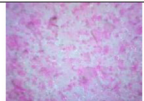
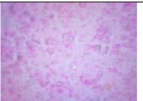
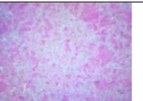
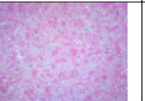
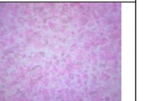
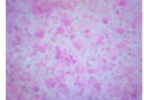
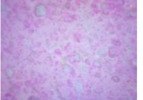
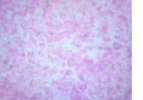

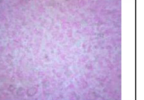
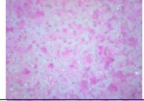
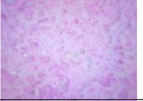

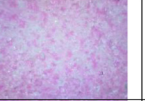
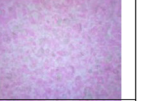
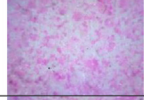
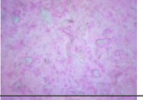
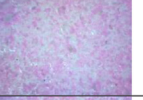

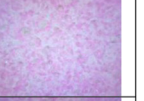
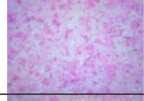
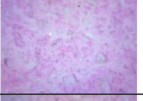
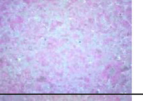
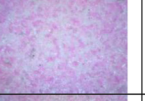
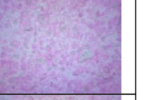
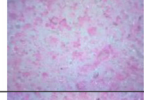
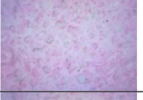
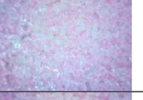
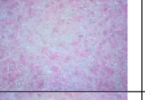
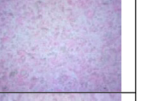
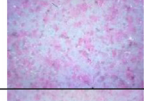
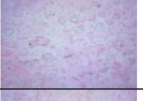
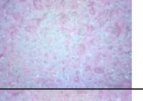
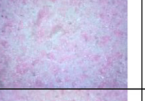
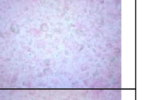
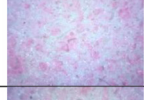

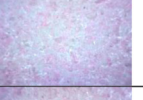

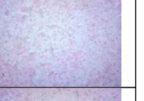
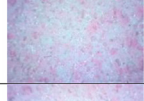
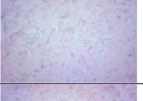
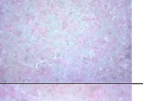
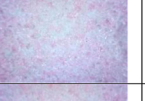
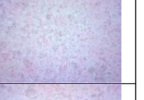
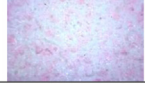
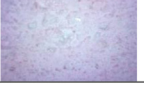
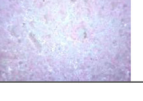
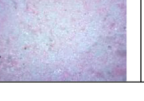

The extremely low reaction rate observed at initial stages, when TiO<sub>2</sub>-Si-Cem mortars were used as photocatalytic cementitious material, represents a marked difference facing TiO<sub>2</sub>-Cem mortars behaviour. A rate decrease was always observed at increasing reaction times when SiO<sub>2</sub> layer was previously coated. The biggest difference was observed for CG13-Si-Cem mortar that practically

stops its photodegradation capacity at fourth day with around 80% molar conversion, meanwhile the TEA coating was the least altered by the insertion of silica layer.

In the attempt to compare both systems: catalyst-coated mortars, TiO<sub>2</sub>-Cem, and catalyst coated on SiO<sub>2</sub>-layered mortars, TiO<sub>2</sub>-Si-Cem; two parameters, half-time photodegradation,  $t_{1/2}$  (see Table 5) defined as the reaction time needed to reach 50% of RhB conversion, and almost total RhB photocatalytic degradation (see Table 6), respectively, were calculated. Both parameters resulted worsened for TiO<sub>2</sub>-Si-Cem mortar samples, what means the difficulty to complete RhB photodegradation when SiO<sub>2</sub> layer was applied in between mortar and catalyst (Table 6), that in some way could be associated with the slowing down suffered during photoreaction evolution as concluded from longer  $t_{1/2}$  presented by TiO<sub>2</sub>-Si-Cem specimens (Table 5). Former results emphasized the need of a photoactivation period that could facilitates the development of hydrophilicity on SiO<sub>2</sub> surface and cross-linking to anchorage layers between them and to the mortar surface, what could improve photoefficiency [47] as revealed the high levels of total conversion reached in spite of the long half-time ( $t_{1/2}$ ) period. In this sense, work in progress will be completed to clarify this point.

**Table 4**

Micrographs of RhB decolouration by photocatalytic degradation on TiO<sub>2</sub> SiO<sub>2</sub> coated cements, obtained at different irradiation times.

Time	Si-Cem	CG1-Si-Cem	CG7-Si-Cem	CG13-Si-Cem	TEA-Si-Cem
0					
30 min					
60 min					
120 min					
240 min					
1 day					
2 days					
3 days					
4 days					
5 days					

**Table 5**

Reaction time needed to obtain 50% of conversion ( $t_{1/2}$ ) on RhB photocatalytic degradation.

	$t_{1/2}$ (min)		$t_{1/2}$ (min)
Cem	4408	Si-Cem	1350
CG1-Cem	70	CG1-Si-Cem	1225
CG7-Cem	48	CG7-Si-Cem	1110
CG13-Cem	618	CG13-Si-Cem	1020
TEA-Cem	72	TEA-Si-Cem	1200

### 3.3. NO<sub>x</sub> photodegradation

NO<sub>x</sub> photodegradation runs were carried out using catalyst coated mortars, due to no improvement on photocatalytic efficiency was achieved when SiO<sub>2</sub> layer was inserted in between catalyst and mortar during RhB dye photodegradation. The curves of NO<sub>x</sub> conversion evolution (Fig. 8) for the four TiO<sub>2</sub>-coated mortars (CG1-Cem, CG7-Cem, CG13-Cem and TEA-Cem) together with the blank (Cem without any coating) show any outstanding differential behaviour among TiO<sub>2</sub> photocatalyst-coated mortars; while

**Table 6**

RhB and NO<sub>x</sub> final conversions on photocatalytic degradation.

	CG1-Cem	CG7-Cem	CG13-Cem	TEA-Cem
RhB (%) <sup>a</sup>	100 ± 5	97 ± 5	98 ± 5	94 ± 5
NO <sub>x</sub> (%) <sup>b</sup>	50 ± 4	52 ± 3	53 ± 3	53 ± 3
	CG1-Si-Cem	CG7-Si-Cem	CG13-Si-Cem	TEA-Si-Cem
RhB (%) <sup>a</sup>	88 ± 5	89 ± 5	81 ± 6	91 ± 5

<sup>a</sup> Calculated after 5 days of irradiation time

<sup>b</sup> Calculated after 1 h of irradiation time



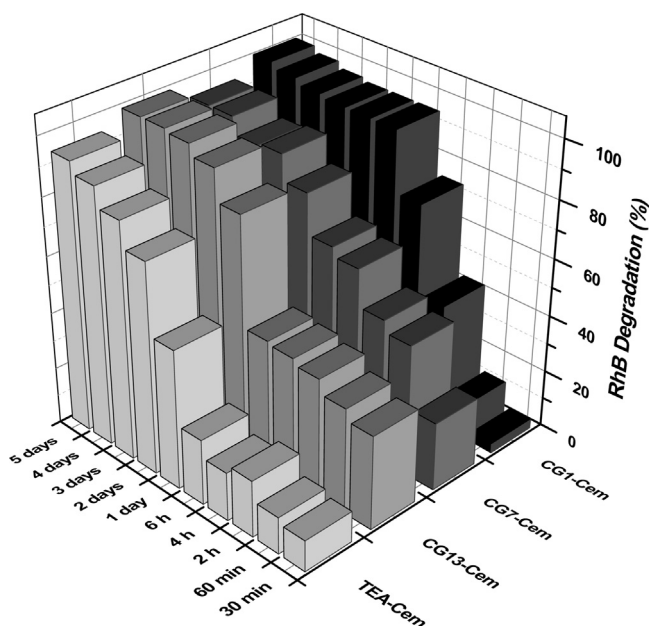


Fig. 6. RhB photodegradation evolution on  $\text{TiO}_2$ -Cem mortars.

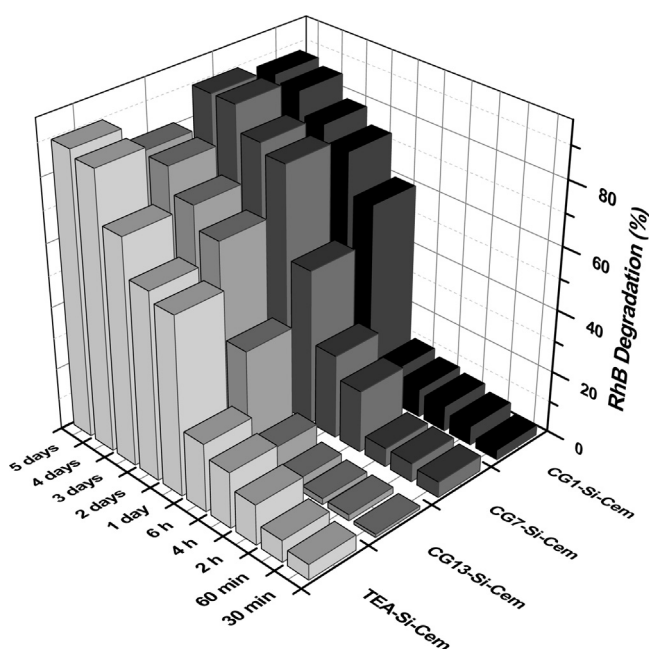


Fig. 7. RhB photodegradation evolution on  $\text{TiO}_2$ -Si-Cem mortars.

the  $\text{NO}_x$  conversion on Cem is negligible just like  $\text{NO}_x$  photoconversion in the absence of catalyst.

The results of total conversion during normalized test of  $\text{NO}_x$  photocatalytic degradation under UNI 11247:2010 conditions showed no significant differences on total conversion among  $\text{TiO}_2$ -Cem samples (Table 6). Although in this case, complete photodegradation never was achieved, provided the type of these test based on a continuous flow passing on the surface of the sample, initial  $\text{NO}_x$  photodegradation rate from time evolution curves observation followed the order: CG7-Cem  $\approx$  CG1-Cem > CG13-Cem  $\approx$  TEA-Cem.

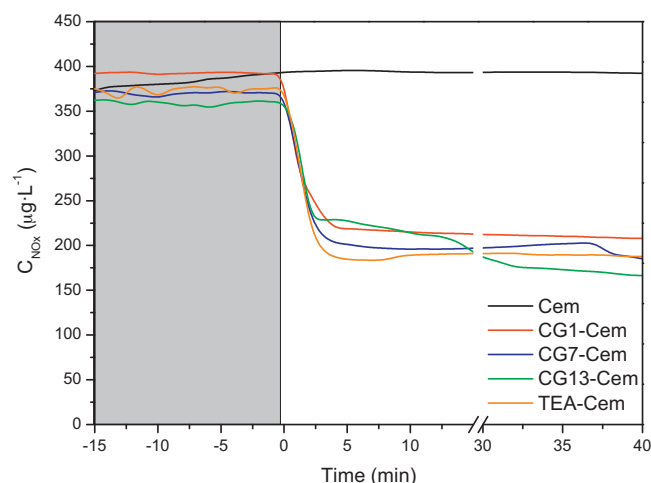


Fig. 8.  $\text{NO}_x$  photodegradation evolution on  $\text{TiO}_2$ -Cem mortars.

#### 4. Conclusions

Concluding, it could be pointed out that all the studied photocatalytic mortars showed a significant activity on RhB and  $\text{NO}_x$  photodegradation, with almost total RhB molar conversions after five days of irradiation and upper 53% for  $\text{NO}_x$  photodegradation in a continuous flow test. Nevertheless, although  $\text{SiO}_2$  layer deposited in between mortar and photocatalysts did not stabilize the commercial  $\text{TiO}_2$  coatings, a good adhesion was observed when applied joint to TEA, probably because of the interactions encountered between  $\text{SiO}_2$  and  $\text{TiO}_2$  sols. A photo-induction period could be necessary to activate  $\text{TiO}_2$ - $\text{SiO}_2$  coatings on mortar surfaces, as a result of the higher halftimes ( $t_{1/2}$ ) differences not corresponding to the total conversions reached.

CG7-Si-Cem exhibited high rate at shorter irradiation times, but TEA-Cem and TEA-Si-Cem can be considered as very interesting and potential photocatalytic mortars due to improved coatings adhesion that provides promising outdoor uses, and acceptable photo-efficiencies in RhB and  $\text{NO}_x$  photo-oxidation.

#### Acknowledgements

This work has been supported by the Spanish Plan National I+D+I through the project CTM2010-14883/TECNO.

#### References

- [1] M.M. Ballari, Q.L. Yu, H.J.H. Brouwers, Catal. Today 161 (17) (2011) 175–180.
- [2] EU Council Directive 1999/30/EC. Relating to Limit Values for Sulphur Dioxide, Nitrogen.
- [3] P. Avila, A. Bahamonde, J. Blanco, B. Sanchez, A.I. Cardona, M. Romero, Appl. Catal. B 17 (1998) 75–88.
- [4] WHO, Air quality guidelines, Global Update 2005, World Health Organization, 2005.
- [5] S. Malato, P. Fernandez-Ibañez, M.I. Maldonado, J. Blanco, W. Gernjak, Catal. Today 147 (1) (2009) 1–59.
- [6] M.M. Ballari, M. Hunger, G. Hüsken, H.J.H. Brouwers, Appl. Catal. B 95 (2010) 245–254.
- [7] M.M. Hassan, H. Dylla, L.N. Mohammad, T. Rupnow, Constr. Build. Mater. 24 (8) (2010) 1456–1461.
- [8] J. Zhao, X. Yang, Build. Environ. 38 (2003) 645–654.
- [9] H. Omisi, S. Rahighi, X. Jiang, Y. Nemoto, A. Beitollahi, S. Wakatsuki, Y. Yamauchi, Chem. Asian J. 5 (2010) 1978–1983.
- [10] F. Pacheco-Torgal, S. Jalai, Constr. Build. Mater. 25 (2011) 582–590.
- [11] D. Lin, K. Lin, W. Chang, H. Luo, M. Cai, Waste Manage. 28 (2008) 1081–1087.
- [12] X. Fu, L.A. Clark, Q. Yang, M.A. Anderson, Environ. Sci. Technol. 30 (1996) 647–653.
- [13] K. Shimazaki, N. Suzuki, N. Miyamoto, Y. Yamauchi, J. Nanosci. Nanotechnol. 11 (2011) 3256–3264.

- [14] Y. Li, B.P. Bastakoti, M. Imura, S.M. Hwang, Z. Sin, J.H. Kim, S.X. Dou, Y. Yamuchi, *Chem. Eng. J.* 20 (2014) 6027–6032.
- [15] L. Pinho, M.J. Mosquera, *Appl. Catal. B: Environ.* 134–135 (2013) 205–221.
- [16] J. Vera-Agullo, V. Chozas-Ligero, D. Portillo-Rico, M. Garcia-Casas, A. Gutierrez-Martinez, J. Mieres-Royo, *Mortar and Concrete Reinforced with Nanomaterials. Nanotechnology in Construction 3*, Germany, Springer, Berlin, Heidelberg, 2009, ISBN 978-3-6-42-00979-2.
- [17] J. Chen, C.-S. Poon, *Build. Environ.* 44 (2009) 1899–1906.
- [18] C.L. Bianchia, C. Pirola, E. Selli, S. Biella, *J. Hazard. Mater.* 211–212 (2012) 203–207.
- [19] A. Folli, U.H. Jakobsen, G.L. Guerrini, D.E. Macphee, *J. Adv. Oxid. Technol.* 12 (1) (2009) 126–133.
- [20] O. Carp, C.L. Huisman, A. Reller, *Prog. Solid State Chem.* 32 (1–2) (2004) 33–177.
- [21] A.M. Ramirez, K. Demeestere, N. De Belie, T. Mäntylä, E. Levänen, *Build. Environ.* 45 (4) (2010) 832–838.
- [22] H. Wang, Z. Wu, W. Zhao, B. Guan, *Chemosphere* 66 (2007) 185–190.
- [23] H. Yaghoubi, N. Taghavinia, E.K. Alamdari, *Surf. Coat. Technol.* 204 (2010) 1562–1568.
- [24] K.O. Awitor, A. Rivatton, J.L. Gargette, A.J. Down, M.B. Johnson, *Thin Solid Films* 516 (2008) 2286–2291.
- [25] T. Moskalewicz, A. Cyriska-Filemonowicz, A.R. Boccacini, *Surf. Coat. Technol.* 201 (2007) 7467–7471.
- [26] M. Okuya, K. Nakade, S. Kaneko, *Sol. Energy Mater. Sol. Cells* 70 (2002) 425–435.
- [27] I. Saeki, N. Okushi, H. Konno, R. Furuichi, *J. Electrochem. Soc.* 143 (1996) 2226–2230.
- [28] A. Brevet, F. Fabreguette, L. Imhoff, M.C. Marco, O. de Lucas, L. Saviot Heintz, M. Sacilotti, S. Bourgeois, *Surf. Coat. Technol.* 151–152 (2002) 36–41.
- [29] K.Y. Jung, S.B. Park, *J. Photochem. Photobiol. A: Chem.* 127 (1999) 117–122.
- [30] Q. Xu, M.A. Anderson, *J. Mater. Res.* 6 (1991) 1073–1081.
- [31] F.U. Xianzhi, L.A. Clark, Q. Yang, M.A. Anderson, *Environ. Sci. Technol.* 30 (1996) 647–653.
- [32] R. Jenkins, R.L. Zinder, *Introduction to X-Ray Power Diffractometry*, John Wiley & Sons Inc., New York, 1996.
- [33] J. Tauc, R. Grigorovici, A. Vancu, *Phys. Stat. Solidi* 15 (1966) 627–637.
- [34] N. Serpone, D. Lawless, R. Khairutdinov, *J. Phys. Chem.* 99 (1995) 16646–16654.
- [35] A. Testino, I.R. Bellobono, V. Buscaglia, C. Canevali, M. D'Arienzo, S. Polizzi, R. Scotti, F. Morazzoni, *J. Am. Chem. Soc.* 129 (2007) 3564–3575.
- [36] UNI 11259:2008, *Determination of The Photocatalytic Activity Of Hydraulic Binders – Rodamina Test Method*, Italian Standards, 2008.
- [37] K. Yu, S.G. Yang, H. He, C. Sun, C.G. Gu, Y.M. Ju, *J. Phys. Chem. A* 113 (2009) 10024–10032.
- [38] X.F. Hu, T. Mohamood, W.H. Ma, C.C. Chen, J.C. Zhao, *J. Phys. Chem. B* 110 (51) (2006) 26012–26018.
- [39] Z. He, C. Sun, S.G. Yang, Y.C. Ding, H. He, Z.L. Wang, *J. Hazard. Mater.* 162 (2009) 1477–1486.
- [40] F.C. Jentoft, *Adv. Catal.* 52 (2009) 129–211.
- [41] UNI 11247:2010, *Determination of the Degradation of Nitrogen Oxides in the Air by Inorganic Photocatalytic Materials: Continuous Flow Test Method*, Italian Standards, 2010.
- [42] C. Kaewtip, K. Accnit, N. Chaowai, K. Areerat, P. Reanjaruan, V. Boonnumnauyvitaya, *Adv. Mater. Phys. Chem.* 2 (2012) 40–44.
- [43] F. Rouquerol, J. Rouquerol, K. Sing, *Adsorption by Powders & Porous Solids. Principles, Methodology and Applications*, Academic Press, San Diego, 1999.
- [44] J. Sekulic, A. Magraso, J.E. ten Elshof, A.D.H. Blank, *Microporous Mesoporous Mater.* 72 (2004) 49.
- [45] Y. Hu, H.L. Tsai, C.L. Huang, *Mater. Res. Eng. A* 344 (2003) 209.
- [46] H. Okochi, H. Kameda, S.I. Hasegawa, N. Saito, K. Kubota, M. Igawa, *Atmos. Environ.* 34 (2000) 2937–2945.
- [47] H.A. van der Sloot, *Cem. Concr. Res.* 30 (2000) 1079–1096.
- [48] Z.Z. Qiang, *Adv. Mater. Res.* 790 (2013) 320–323.
- [49] J. Chen, C.S. Poon, *Environ. Sci. Technol.* 43 (2009) 8948–8952.
- [50] J.M. Wu, T.W. Zhang, *J. Photochem. Photobiol. A: Chem.* 162 (1) (2004) 171–177.
- [51] M. Asilturk, F. Sayilkan, S. Erdemoglu, M. Akarsu, H. Sayilkan, M. Erdemoglu, E. Arpac, *J. Hazard. Mater.* 129 (1–3) (2006) 164–170.
- [52] T. Yuranova, V. Sarria, W. Jardim, J. Rengifo, C. Pulgarin, G. Trabesinger, J. Kiwi, *J. Photochem. Photobiol. A: Chem.* 188 (2007) 334–341.
- [53] E. Quagliarinia, F. Bondiolib, G.B. Goffredoa, A. Licciulli, P. Munafò, *J. Cult. Herit.* 14 (2013) 1–7.
- [54] S.M. Melpolder, A.W. West, C.L. Bauer, *MRS Proc.* 239 (1991) 371–375.
- [55] A. Fujishima, X. Zhang, C. R. Chim. 9 (2006) 750–760.
- [56] A. Maury, N. De Belie, *Mater. Constr.* 60 (298) (2010) 33–50.